Neural-Sliding Mode Augmented Robust Controller for Autolanding of Fixed Wing Aircraft

Shaik Ismail, Abhay A. Pashilkar
Scientists, Flight Mechanics and Control Division, CSIR-National Aerospace Laboratories
Bangalore – 560017, India
shaik1752@gmail.com, apash@nal.res.in

Ramakalyan Ayyagari
Prof., Dept. of Instrumentation and Control Engg., National Institute of Technology
Tiruchirappalli, India

N. Sundararajan
Professor, School of Electrical & Electronic Engineering, Nanyang Technological University,
Singapore 639798

May 23, 2013

Abstract Neural and sliding mode controllers are generally based on the principle of nonlinear dynamic inversion. This leads to control signals containing high frequency components. This can result in actuator rate limiting due to loss of phase at higher frequencies. Large control inputs, for example due to the saturation component of the sliding mode controller can also result in position saturation of the actuator. In this paper we show that by the introduction of suitable phase compensators and an anti-windup scheme the neural-aided sliding mode controller performance can be improved. A novel scheme is proposed for the cascaded feedback controller which addresses practical requirements of both state limiting and control surface saturation respectively.

1 Introduction

Neural control [1-6] is a popular approach to introduce learning or adaptation in control systems. This is due to the universal approximation properties of a neural network. Sliding mode control [7-9] also has been widely studied due to the desirable property of these controllers to reach the sliding manifold in finite time. However, it is known that these two approaches are based on Nonlinear Dynamic Inversion (NDI) principles. NDI controllers are known to be non-robust to parameter uncertainties in general as they involve cancellation of nonlinearities. Therefore, most designers use appropriate feedback loops within their neural and sliding mode controllers to enhance robustness. They also use feedback errors for online learning to achieve good cancellation of the nonlinearities over a period of time.

In passing we mention some other control strategies like L_1-adaptive control [10] and integrator backstepping [11]. L_1-adaptive control is based on the concept that the controller should only attempt to control the plant within the bandwidth of the control channel. A low-pass filter is placed in the control channel. Thus, the L_1-adaptive control architecture decouples adaptation from the robustness of the system and also provides performance bounds for both the input and output of the plant. However, designing suitable low-pass filters and state predictors is a laborious process. Further, in the case of unknown actuator failures, recourse is made to neural-networks to model nonlinearities and control effectiveness.

The backstepping method uses a recursive synthesis procedure to determine nonlinear

controller for linear or nonlinear systems with particular cascaded structure. Backstepping improves the robustness of the controller by introducing feedback of the virtual controls into the cascaded structure. In [11] the authors have applied backstepping with the assumption that the slow dynamic characteristic is accurately known. The robustifying (namely the saturation) term for these controllers can cause rate and position saturation. This requirement is relaxed in [12], and backstepping is applied assuming all subsystems in the cascaded controller have uncertainties. However, by foregoing the time-scale separation assumption, the neural networks are now not only a function of the state variables at each stage but also the gradients of the virtual controls with respect to the state variables. Further, the gains multiplying the error state variables are also time varying. This makes the implementation of the controller complex. In this paper we overcome the problem of actuator position and rate saturation by introducing anti-windup and phase compensation respectively.

This paper aims to demonstrate that the adverse effects of high bandwidth or abrupt large inputs which cause actuator rate and position limiting can be handled for neural-aided and sliding model controllers developed by the authors [8, 13] using phase compensating filters developed for pilot-induced oscillations [14] and anti-windup strategies [15]. The position and rate saturation in the actuators, which are typically not inverted in the dynamic inversion process for neural and sliding mode control leads to the presence of “holes” or gaps in the fault tolerance range or envelope of the controllers [8, 13]. The phase compensating filters are used to mitigate the effect of actuator rate saturation, while the anti-windup is used to prevent over-driving the actuators when they are in position saturation. A novel type of anti-windup scheme is proposed for the cascaded feedback controller with multiple redundant control surfaces which addresses both state and control surface saturation.

The rest of the paper is organized as follows: The autolanding problem and the aircraft model is discussed in Section 2. A brief description of the failure scenarios is also provided in this section. The design on the fault tolerant controller is discussed in Section 3, while the simulation results are presented in Section 4. Finally, the conclusions drawn from this study and the plans for future work are given in the final section.

2 Autolanding Problem Formulation

The autolanding trajectory (Fig. 1) consists of segments such as wings-level flight at 600 m altitude, two coordinated level turns, glide slope descent and finally the flare maneuver and touchdown on the runway. The first turn segment serves to train the neural networks online. Actuator failures are injected just before the second turn.

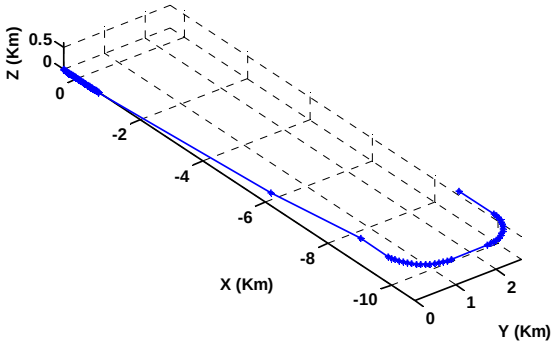

Figure 1: Landing trajectory.

2. 1 Aircraft Model

The mathematical model of the aircraft chosen for the study is that of a high performance fighter aircraft with conventional control surfaces, but with independent left and right elevator and aileron controls. Additional aerodynamic data for the split elevator and aileron control surfaces was generated using Computational Fluid Dynamics (CFD) [16]. The two elevators have a deflection range of -25 to + 25 deg. The deflection range for the independent ailerons is -20 to +20 deg., and for the rudder it is -30 to +30 deg.

2.2 Actuator Models and Failure Scenarios

The hydraulic actuators are modeled as first order lags with a time constant of 50millisec, and a rate limit of 60 deg/s. In the present study six types of actuator failures are considered: failure of left elevator alone, failure of either left or right aileron alone, combined failure of left elevator and left aileron, combined failure of left elevator and right aileron, combined failure of both the ailerons, and failure of rudder alone. Failure of

both the elevators is not considered because this case is, in general, not recoverable.
Failure of actuators can occur at any time during the flight. In the present study failures were injected just before the two critical stages of the landing flight: level turn and descent phases. Further, the failed control surfaces can be stuck at any value within the permissible range of deflections.

2.3 Wind Profiles

The wind disturbances are assumed to be present along all the axes throughout the landing mission, and are modeled on Dryden spectrum as shown in Fig. 2 along the x-earth axis. A microburst wind profile is simulated along the other two earth fixed axes.

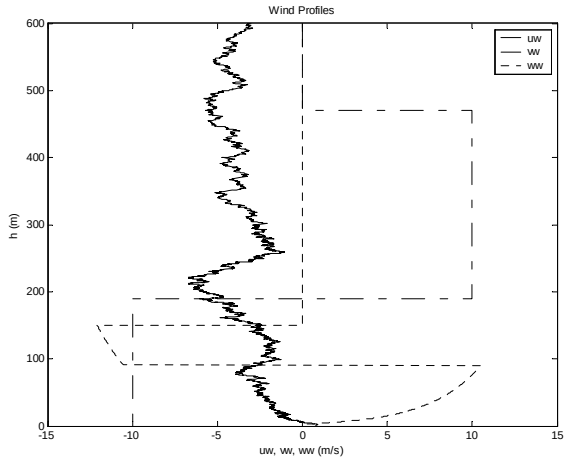

Figure 2: Wind profile during autolanding.

2.4 Safety and Performance Criteria

The runway threshold ($x = y = z = 0$) is treated as the desired touchdown point of aircraft. Since the ideal touchdown cannot be achieved under unknown actuator failures, some safety and performance criteria are checked if the aircraft touches down successfully:

- X-distance and Y-distance: $-100m \le x \le 400m$, $-5m \le y \le 5m$, to restrict the landing area to a rectangle of $500\text{m} \times 10\text{m}$, also called as "Pillbox".
- Total velocity: $V_T \ge 60m/s$ to prevent stall
- Sink rate: $\dot{h} \ge -2m/s$, to prevent landing gear damage
- Bank angle: $|\phi| \le 10\deg$, to prevent wing tips touching the ground
- Heading angle error: $|\psi| \le 15\deg$, to prevent excessive side loads on landing gear

2.5 Fault Tolerance Feasibility Regions

The feasible domain of failures does not coincide with the full range of control surface deflections because in some cases the resulting moments cannot be trimmed out for the landing maneuver. Thus, the full range of hard over positions must be checked for the feasible subset. This set is a union of the following trim computations:

- Region of level flight trim: body axis rates and flight path angle $p = q = r = \gamma = 0$, 6 DOF accelerations = 0
- Region of level descent trim: body axis rates $p = q = r = 0$, flight path angle $\gamma = -6\deg$, 6 DOF accelerations=0
- Region of level turning trim: bank angle $\phi = 40\deg$, 6 DOF accelerations=0.

3 Controller Implementation

The philosophy behind the design of the autolanding controller discussed in this paper can be illustrated using the ideas inherent in the Sliding Mode Control (SMC) concept. An affine plant can be represented by

$$\dot{x} = f(x) + bu \tag{1}$$

where, $x \in R$ is the state vector and $u \in R$ is the control input. It is assumed that the function $f(x)$ is unknown, and the scalar b does not change sign in the state space. Let the sliding mode surface be given by

$$S = \tilde{x} + \lambda \int_0^t \tilde{x}\, d\tau \tag{2}$$

where, $\tilde{x} = x - x^d$ is the state error, with x^d being the desired trajectory. The gain λ is a positive number physically representing the

bandwidth of a filter, and it is chosen to satisfy the Lyapunov stability criteria.

The sliding mode control law is composed of two modes. The first mode is a reaching mode where the states beginning from arbitrary state are attracted towards the sliding surface $S = 0$. The state error $\tilde{x}$ conveges to zero because $S = 0$. In the second mode, the states slide along the sliding surface. The time derivative of sliding surface is given by

$$\begin{aligned} \dot{S} &= \dot{\tilde{x}} + \lambda \tilde{x} = \dot{x} - \dot{x}^d + \lambda \tilde{x} \\ &= f(x) + bu - \dot{x}^d + \lambda \tilde{x} \end{aligned} \tag{3}$$

To satisfy $\dot{S} = 0$ on the sliding surface, the equivalent control is given by

$$u_{eq} = \frac{1}{b}\left\{ \dot{x}^d - \lambda \tilde{x} - f(x) \right\} \tag{4}$$

Once the state trajectory reaches the sliding surface $S = 0$, the equivalent control guarantees that the trajectory remains in the sliding surface under the ideal condition. When the state is outside the sliding surface, the controller must drive the system state trajectory to the switching surface and maintain the sliding mode condition. Thus, SMC is a variable structure controller of the form

$$u = u_{eq} + u_s \tag{5}$$

where, u_s is a switching control expressed as

$$u_s = K \,\mathrm{sign}(S), \text{ with } K > 0 \tag{6}$$

To reduce chattering, due to discontinuous behaviour, the sign function is usually replaced by the saturation function

$$u_s = K \,\mathrm{sat}(S), \quad K > 0 \tag{7}$$

where the saturation function is defined as

$$sat(S) = \begin{cases} 1 & if \quad S > \varepsilon \\ -1 & if \quad S < -\varepsilon \\ 0 & if \quad -\varepsilon \le S \le \varepsilon \end{cases} \tag{8}$$

where ε is the thickness of a thin boundary layer neighbouring the sliding surface.

It is worthwhile to reflect on the structure of the sliding mode control derived above.

$$\begin{aligned} u &= \frac{1}{b}\left\{ \dot{x}^d - \lambda\tilde{x} - f(x) \right\} + K\, sat(S) \\ &= -\frac{1}{b}\lambda\,\tilde{x} + \frac{1}{b}\left\{ \dot{x}^d - f(x) \right\} + K\, sat(S) \\ &= u^{FC} + u^{INV} + u^{SAT} \end{aligned} \tag{9}$$

In the above equation, we view the first term as a classical feedback controller. The second term could be a Nonlinear Dynamic Inversion (NDI) controller. In our case, we will use the Extended Minimal Resource allocation Network (EMRAN) neural controller, with online learning which is based on Radial Basis Functions (RBF) [17]. Finally, the third term is the saturation control which fires when the error exceeds the error threshold around the sliding surface. The selection of numerical values for the parameters λ and K is discussed in the section dealing with controller design.

A similar concept of using a classical feedback controller, a neural controller and a saturation controller for accommodating actuator failures s given in [9]. The total control signal is given as [9]:

$$u(t) = u^{PID} + (1 - m(t))u^{INV} + m(t)u^{SAT} \tag{10}$$

where u^{PID} is the feedback term from a PID controller, u^{INV} is the neural network control output, u^{SAT} is saturation controller output, and $m(t)$ is a modulation function varying beteween zero and unity. The modulation function determines the contribution of neural controller and saturation controller to the complete control law. Thus, the complete control law has a dual charater, acting either as a sliding or an an adaptive neural controller depending upon the instantaneous state error. This avoids discontinuously switching between the neural-adaptive and sliding components. However, RBF network has fixed parameters, and hence restricted fault-tolerance capability. In the controller discussed in this paper, a fully tuned neural network (EMRAN) is used which expands the fault-tolerance range of the controller.

The controller resulting from the concept of Eq. (9) is is shown in Fig. 3. The outermost loop is the tracking controller which computes the desired ground track angle, lateral deviation from the desired trajectory, desired velocity and the desired altitude.

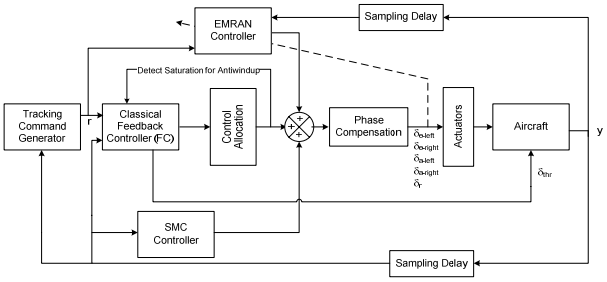

Figure 3: Schematic of neural sliding mode controller.

3.1 Feedback Controller (FC)

The classical feedback controller (FC) is designed separately for the longitudinal axis (Fig. 4) and lateral-directional axis (Fig. 5).

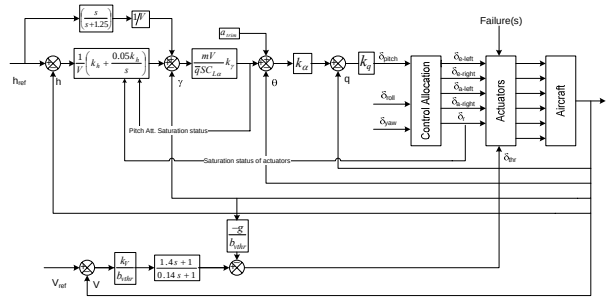

Figure 4: Longitudinal axis feedback controller.

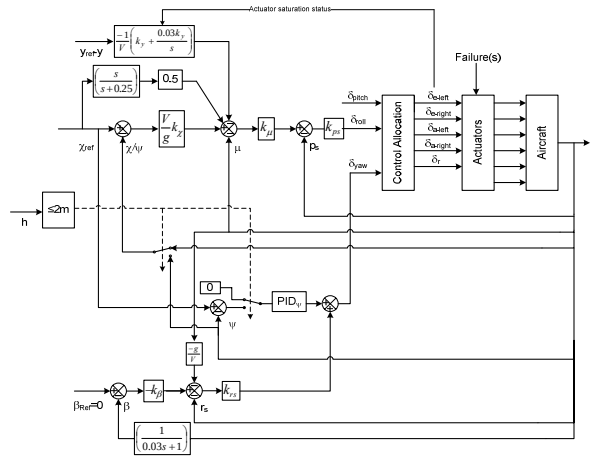

Figure 5: Lateral-directional axis feedback controller.

The feedback controller is designed for the nominal plant. Its gains are chosen such that when there are no failures or winds the innermost feedback loop do not cause rate or position limiting of the actuators. The pitch rate gain is given by $K_q = -\lambda/b$, and a value of -105 was obtained for this gain. Similarly, the roll rate gain K_{ps} is chosen as -20.

Multiple surface redundancy is used to enhance the ability of the controller to handle failures. For example, both ailerons failed case is handled by using the independent elevator control surfaces in differential mode for the control of roll and yaw:

$$\begin{bmatrix} \delta_{e-left} \\ \delta_{e-right} \\ \delta_{a-left} \\ \delta_{a-right} \\ \delta_{rudder} \end{bmatrix} = \begin{bmatrix} 1.0 & -0.75 & -0.27 \\ 1.0 & 0.75 & 0.27 \\ 0 & -1.0 & 0 \\ 0 & 1.0 & 0 \\ 0 & 1.66 & 1.0 \end{bmatrix} \begin{bmatrix} \delta_{pitch} \\ \delta_{roll} \\ \delta_{yaw} \end{bmatrix} \quad (15)$$

The gain entry of 1.66 is the aileron to rudder interconnect. The entries ± 0.75 represent the use of elevators in differential mode to achieve control in the roll axis. This gain allows us to tolerate the additional failure case where both ailerons failed. Similarly, the gain entries ± 0.27 are intended to create differential elevator control in response to demand for control in the yaw axis and enhance the ability of the FC to handle rudder failures.

To protect against integrator windup, control surface saturation is detected. The control allocation matrix in (4) means that for example if the left elevator is saturated, it could be due to either the pitch, roll or yaw axis control signals. Therefore, in this case we hold the integrators in all the three axes for the duration for which the left elevator is saturated. This way we prevent the control system from overdriving the actuators.

It is also seen that the limits on the state variables like pitch attitude is also incorporated in the pitch axis integrator. The general principle for the anti-windup design is that any state or control surface saturation in the inner loops of the cascaded controller should result in the integrators in the loops outer to be held for the duration of the time the variable is in saturation. This general anti-windup scheme addresses both state and control surface saturation for a cascaded controller structure.

3.2 EMRAN Controller

The EMRAN is a fast implementation of the Radial basis Function neural network [17] where only the nearest neuron is updated each

cycle. A brief description of EMRAN is given here. More details can be found in [17].

The outputs of RBF network with Gaussian function Φ are given by

$$f(\xi_n) = a_0 + \sum_{i=1}^{h} \Phi_i(\xi_n),\ \xi \in R^m,\ f \in R^p \quad (16)$$

where

$$\Phi_i(\xi_n) = \alpha_i \exp\left(-\frac{1}{\sigma_i^2} \|\xi_n - \mu_i\|^2 \right) \quad (17)$$

and, ξ is the input vector of the network, h indicates the total number of hidden neurons, μ_i and σ_i refer to the centre and width of the i^{th} hidden neuron respectively, n is the time index, and $\|\ \|$ is the Euclidean norm. The function f is the output of RBF network, which represents the network approximation to the desired output y_n. The coefficient α_i is the connection weight of the i^{th} hidden neuron to the output layer and a_0 is the bias term and both are vectors.

The network starts with no hidden neurons. As input data ξ_n and corresponding output data pair y_n is received sequentially, the network adds or prunes hidden neurons based on the following three steps [17]:

1. Calculate the network outputs based on current inputs and determine the following errors:

$$\|e_n\| = \|y_n - f(\xi_n)\| > E_1 \quad (18)$$

$$e_{rmsn} = \sqrt{\sum_{i=n-(M-1)}^{n} \|e_i\|^2 \Big/ M} > E_2 \quad (19)$$

$$d_n = \|\xi_n - \mu_{nr}\| > \max\left(e_{\max} r^n, e_{\min}\right) \quad (20)$$

where $E_1, E_2, e_{\max}, e_{\min}$ are thresholds to be selected *a priori*, while $0 < r < 1$ is a decay factor, μ_{nr} is the centre of the hidden neuron that has the closest distance to ξ_n.

2. If all of the error criteria in (18)-(20) are satisfied, add a new hidden neuron. When a new neuron is added, the associated parameters are fixed using the following rules:

$$\mu_{h+1} = \xi_n,\ \sigma_{h+1} = \kappa\|\xi_n - \mu_{nr}\|,\ \alpha_{h+1} = e_n \quad (21)$$

3. If any of the error criteria in (18)-(20) are not met, adjust the parameters w of the existing RBF network using the Extended Kalman Filter (EKF), where

$$w = \left[\alpha_0^T, \alpha_1^T, \mu_1^T, \sigma_1, ..., \alpha_h^T, \mu_h^T, \sigma_h^T\right] \quad (22)$$

EMRAN differs from the MRAN in this last step. Instead of updating all the parameters (representing weights, centers and widths) of all the hidden neurons, it only updates the parameters of the neuron nearest to the input data vector. There is only slight difference between the performance of EMRAN and MRAN in terms of approximation error but in terms of speed EMRAN outperforms MRAN significantly.

The original EMRAN also incorporates a pruning strategy which is not used in this implementation. The EMRAN controller design consists of finding suitable values of parameters $E_1, E_2, e_{\min}, e_{\max}, r, \kappa, p_0, q_0, r_0$.

Now, consider the aircraft dynamics represented by the equations

$$\dot{x} = f(x,u) \quad (22)$$

with f assumed to be smooth and having bounded first derivatives in the neighborhood of the trajectory. The inversion may be represented by the equations:

$$u = f^{-1}(\dot{x}, x) \quad (23)$$

where f^{-1} represents the inversion of the equations of motion. Next, this set of multivariable functions are synthesized using the states and their derivatives to obtain the control inputs required to make the aircraft follow the desired trajectory. Further, if this function representing the inverse aircraft dynamics is changing over a period of time, we can exploit the learning ability of the neural network to generate immediate corrective action when such changes take place.

With this as the motivation, the total controller output as the signal to be learned by EMRAN. Over a period of time EMRAN learns the total control signal which results in driving the FC+SMC control output to zero. This means that EMRAN has generated the inverse of the

plant by learning the inverse functions represented by $u = f^{-1}(\dot{x}, x)$.

Figure 6 shows the combined longitudinal and lateral-directional EMRAN block. It is noted that the state variables have been scaled by the linear derivatives. This is intended to improve the numerical conditioning of the inputs to this block.

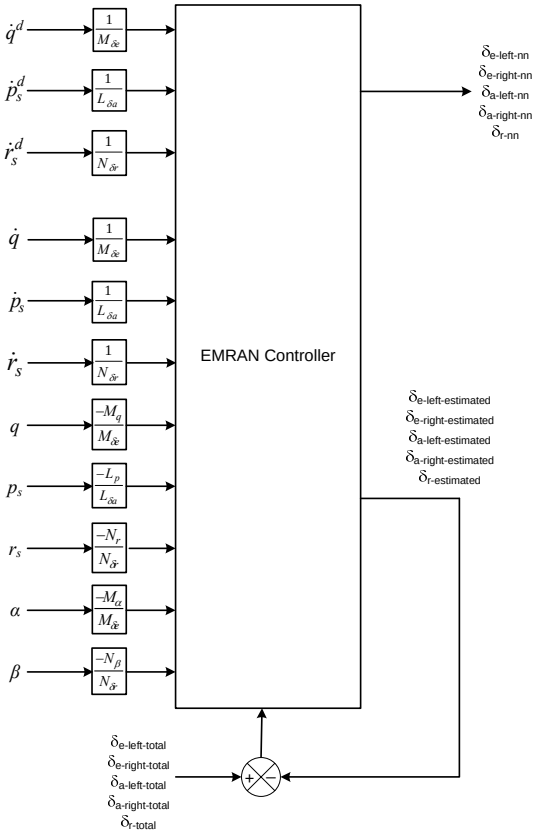

Figure 6: EMRAN controller block schematic.

3.3 Sliding Model Controller

The saturation control of the sliding mode controller comes into play only if the error exceeds a threshold. The saturation control is designed to act rapidly once a stuck actuator failure results in an error exceeding this threshold. This is aimed at preventing the aircraft from seeing large transients and permitting EMRAN controller to learn at a moderate rate. Using simulation of typical actuator failure cases, the gain K of the saturation control is chosen to be a fraction of the maximum deflection of the control surface such that it does not lead to actuator rate saturation, but effectively aids the feedback controller in fault-tolerance. This is the only gain which was chosen by trial and error. The other gain λ is obtained by solving the equality $K_q = -\lambda / b$, where b is the linear control effectiveness derivative.

3.4 Phase Compensator

The SAAB phase compensator is designed specifically to reduce the phase lag due to rate limiting. The schematic of the compensator is shown in Fig. 7.

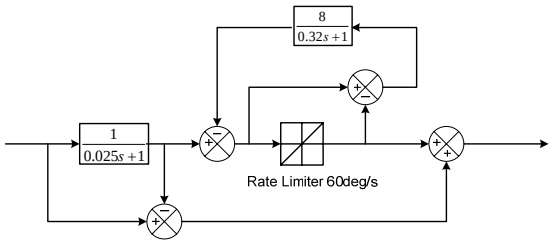

Figure 7: SAAB phase compensator for alleviation of actuator rate limiting.

The tuned values for this filter give better phase response when placed ahead of the actuator. The frequency response of the phase compensated actuator is shown in Fig. 8.

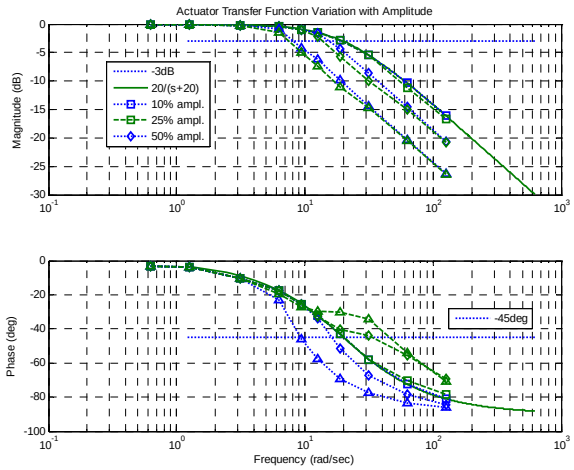

Figure 8: Amplitude dependent response of actuator (dotted lines: without compensator, dashed lines: with phase compensator).

4 Results

In [13], we compared the results for classical Feedback Controller (FC) alone with that for the FC+EMRAN+SMC controller. It was found that the failure tolerance envelope of the FC was nearly the same or better when compared to that for the FC+EMRAN+SMC. In fact the latter controller had a smaller envelope for the two aileron failure case.

Examination of these cases indicated that the primary cause for the performance degradation was the actuator rate or position limiting.

The use of anti-windup and phase compensation filter in the command path for each of the aerodynamic control surfaces was evaluated. We find that with these compensations, the FC+EMRAN+SMC controller has nearly the same or better performance compared to the controller without compensation. To illustrate this, we present two cases, namely a) left elevator failure and b) both aileron failure case in Fig. 9-10 respectively.

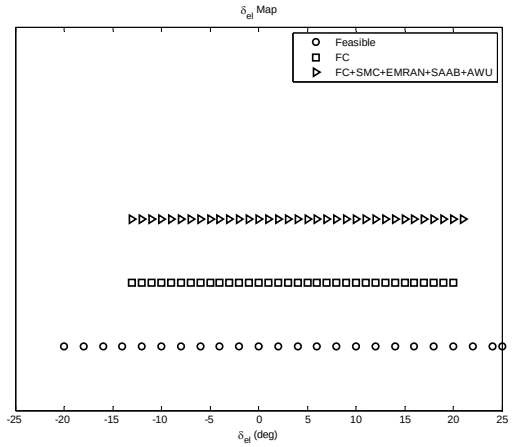

Figure 9: Left elevator failure for FC (open squares) and FC+SMC+EMRAN+SAAB +AWU (open circles).

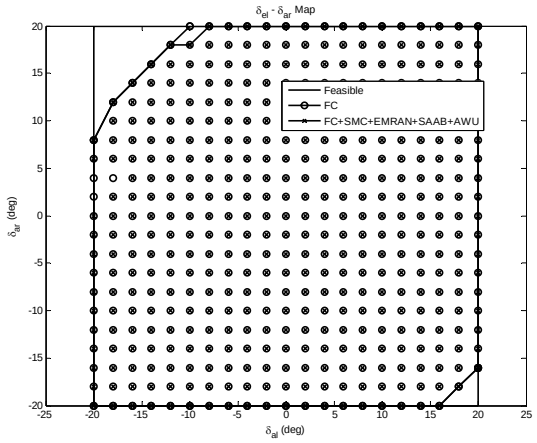

Figure 10: Left aileron-right aileron failure feasibility map for FC (open circle) and FC+SMC+EMRAN+SAAB+AWU (cross).

It is seen from Fig. 9 that the single elevator case is marginally improved due to the phase compensator and anti-windup. In Fig. 11, the result of the FC is compared for FC+EMRAN+SMC (i.e., without the anti-windup and phase advance protection).

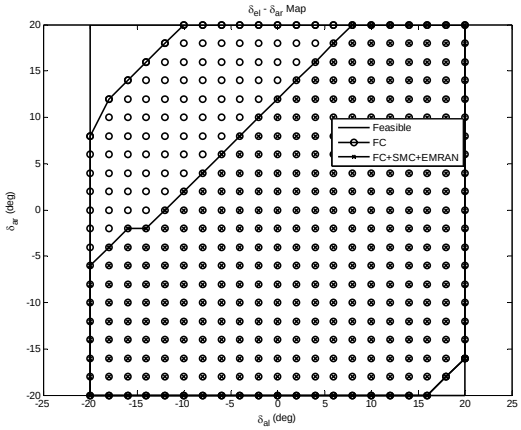

Figure 11: Left aileron-right aileron failure feasibility map for FC (open circles) and FC+SMC+EMRAN (cross).

When we compare this result with Fig. 10, it is immediately clear that adding the anti-windup and phase advance does improve this failure envelope significantly.

Finally in Fig. 12-14, we show the response of the aircraft during a successful landing with the neural-aided sliding mode controller for a three control surface stuck case (left aileron = 2deg, right aileron = -2deg and rudder stuck at 4deg).

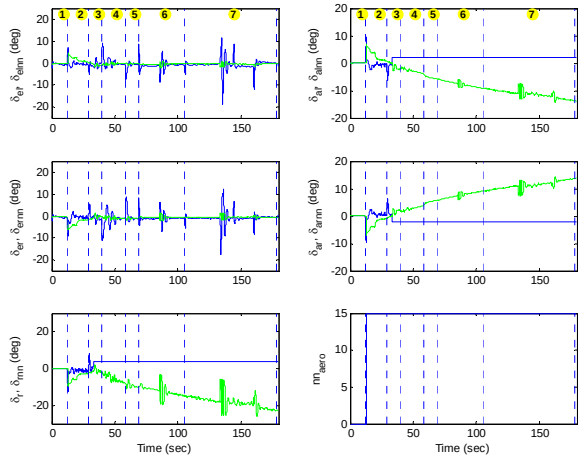

Figure 12: Control surface deflections for a three failure case (left aileron failed to 2deg, right aileron failed to -2deg and rudder failed to 4deg, neural output plotted in green).

Fig. 12 shows the total control surface deflections as well as those computed by the neural network. Fig. 13 and 14 show the longitudinal and lateral-directional response of the aircraft respectively.

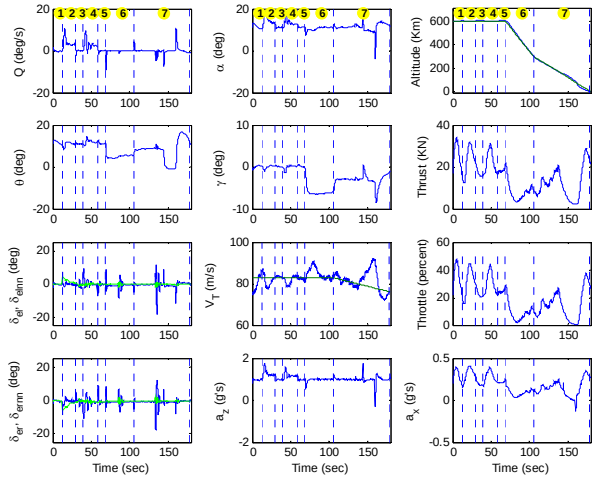

Figure 13: Aircraft response in longitudinal plane for a three failure case (left aileron failed to 2deg, right aileron failed to -2deg and rudder failed to 4deg, neural output plotted in green).

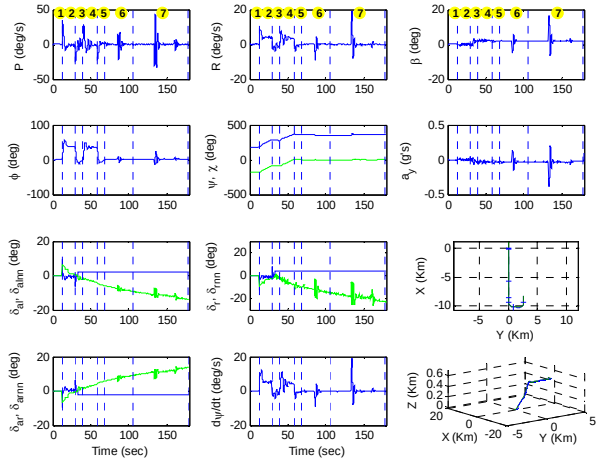

Figure 14: Aircraft response in lateral plane for a three failure case (left aileron failed to 2deg, right aileron failed to -2deg and rudder failed to 4deg, neural output plotted in green).

Conclusion

A neural-aided sliding mode controller design has been studied with regard to its failure tolerance for stuck actuator faults during an autolanding scenario. It is shown that the addition of phase compensation and anti-windup to protect the actuators from rate and position limiting is beneficial to the failure tolerance of this controller. A novel anti-windup scheme is proposed in this paper to handle state and control surface limiting in a cascaded controller with multiple redundant control surfaces. A case of successful landing with three control surfaces failed and stuck is also presented.

References

[1] B. S. Kim, and A. J. Calise., "Nonlinear flight control using neural networks," *Journal of Guidance, Control and Dynamics*, 20(1), 1997.

[2] W. Zhang, "Control of a High Performance Aircraft by Using H_∞ Theory and Neural-Fuzzy Concepts," M. Engg. Thesis, School of EEE, NTU Singapore, 1997.

[3] Y. Li, N. Sundararajan, and P. Sarathchandran, "Neuro-controller design for nonlinear fighter aircraft maneuver using fully tuned RBF networks," *Automatica*, vol. 37, pp. 1293-1301, 2001.

[4] Y. Li, N. Sundararajan, P. Saratchandran, and Z. Wang, " Robust neuro-H_∞ controller design for aircraft autolanding," *IEEE Trans. on Aerospace and Electronic Systems*, vol. 40, no. 1, pp.158-167, January 2004.

[5] A. A. Pashilkar, N. Sundararajan., and P. Saratchandran, "A fault-tolerant neural aided controller for aircraft autolanding," *Aerospace Science & Technology*, vol. 10, pp. 49-61, 2006.

[6] Z. Wang and G. Xiong, "Neuro-aided H_2 controller design for aircraft under actuator failure," *in Proc. of the 2011 2nd Intl. Congress on Computer Applications and Computational Science*, vol. 2, 2011.

[7] H. Alwi, "Fault Tolerant Sliding Mode Control Schemes with Aerospace Applications," Ph.D. Thesis, University of Leicester, UK, 2008.

[8] S. Ismail, A. A. Pashilkar, and R. Ayyagari, "Guaranteed stability and improved performance against actuator failures using neural-aided sliding mode controller for autolanding task," *in Proc. IFAC-EGNAC 2012 Workshop*, IISc Bangalore, 13-15 Feb. 2012.

[9] R. M. Sanner and J-J E. Slotine, "Gaussian Networks for Direct Adaptive Control", *IEEE Trans. on Neural Networks*, vol. 3 no. 6, pp.837-863, November 1992.

[10] V. V. Patel, C. Cao, N. Hovakimyan, K. A. Wise, and E. Lavretsky, "L_1 Adaptive controller for tailless unstable aircraft in the presence of unknown

actuator failures," *Intl. Jl. of Control*, 82(4), 705-720, 2009.

[11] T. Lee and Y. Kim, "Nonlinear adaptive flight control using backstepping and neural networks controller, " *J. Guid., Contr., Dynam.*, 24(4), 2001.

[12] D. -H. Shin, and Y. Kim, "Reconfigurable Flight Control System Design Using Adaptive Neural Networks," *IEEE Trans. on Control System Technology,* 12, 87-100, 2004.

[13] S. Ismail, A. A. Pashilkar, R. Ayyagari and N. Sundararajan, "Improved Autolanding Controller for Aircraft Encountering Unknown Actuator Failures," *in Proc. CISDA 2013,* Singapore, 16-19 April 2013, in press.

[14] G. Hovmark and G. Duus, "Experimental Evaluation of Phase Compensating Rate Limiters in an Aircraft's Lateral Flight Control System", TP-120-04, Group for Aeronautical Research and Technology in Europe, August 2001.

[15] J. Brindley, J. M. Counsell, O. S. Zaher and J. G. Pearce, "Design and simulation of a non-linear, discontinuous, flight control system using rate actuated inverse dynamics", *Proc. IMechE Part G: J. of Aerospace Engineering*, 0(0) 1-15, 2012.

[16] S. G. Teo, Autolanding System Study: Aerodynamic Data on an Aircraft with Independent Control Surfaces by CFD, Technical Report of DSO National Lab., Singapore, 2003.

[17] Y. Li, N. Sundararajan, and P. Saratchandran, "Neuro-flight controllers for aircraft using minimal resource allocating networks (MRAN). *Neural Computing & Applications*, 10, 172-183, 2001.